Case Studies in Thermal Engineering 8 (2016) 250–259

Contents lists available at ScienceDirect

Case Studies in Thermal Engineering

journal homepage: www.elsevier.com/locate/csite

Study on TBCs insulation characteristics of a turbine blade under serving conditions

J.H. Liu [a], Y.B. Liu [a,*], X. He [a], L. Liu [b]

[a] College of Power Engineering, Naval University of Engineering, Wuhan 430033, China
[b] College of Physics Science and Engineering Technology, Yichun University, Yichun 336000, China

ARTICLE INFO

Article history:
Received 10 June 2016
Received in revised form
1 August 2016
Accepted 19 August 2016
Available online 26 August 2016

Keywords:
Thermal barrier coating
Insulation
Coupling
Turbine blade
Temperature fluctuation

ABSTRACT

It is a key problem to study thermal barrier coatings (TBCs) insulation and followed stresses for the coated blade. This article focused on the insulation characteristics of TBCs by coupling heat transfer and flow with a multilayer blade. We found that the coated blade can benefit more in the decline of average temperature than the decline of maximum temperature, compared to the uncoated case. Temperature fluctuation on TBCs surface is evident. The inlet temperature of main flow (T_{in}) more than the heat transfer coefficient of cooling passages (h_{cool}) impacted the fluctuation. And there is a non-homogeneous distribution of the temperature decline (ΔT) across the coatings around the blade. At the suction side and the head, ΔT was generally higher than that of the pressure side and the tail. The TBCs thickness and T_{in} can affect ΔT more than h_{cool}. We suggest that in the sequential TBCs stresses simulation the actual temperature distribution should be prescribed.

1. Introduction

Thermal barrier coatings (TBCs) have been widely used to protect the hot components of the gas turbine, such as combustion, guide vane, and turbine blade, for the low thermal conductivity and well corrosion resistance [1,2]. TBCs normally consists of four layers including top coating (TC), thermally grown oxide (TGO), bond coating (BC), and substrate (SUB). Due to the differences of material properties and harsh environment in service, residual stresses always develops in the layers and result in coatings failure [3]. In the elevated temperature, the oxide diffusion and reaction with the aluminum gradually conduces the TGO growth, which accelerates the coatings failure [4,5]. Thermal mismatch and TGO growth are regarded as the major factors responsible for general failure of TBCs. Many investigations concentrated to explain the failure mechanism after thermal cycles [6–15].

However, the computational models of previous literatures based on the two dimensional periodic unit cannot cover the entire turbine blade geometry and the corresponding working conditions. Ranjbar-far et al. [14,15] built a model of TBCs considering the non-uniform temperature distribution, but the limit of the scale restricted the application to the whole blade.

Finite element method (FEM) has been used for blade heat transfer analysis. Tietz and Koshel [16] simulated three dimensional steady state temperatures distribution of a blade without TBCs using a FEM code. Kumar and Kale [17]

* Corresponding author.
E-mail addresses: ljh363418@sina.cn (J.H. Liu), yongbaoliu@aliyun.com (Y.B. Liu), hexing_mail@163.com (X. He), ll4246@126.com (L. Liu).

http://dx.doi.org/10.1016/j.csite.2016.08.004
2214-157X/

computed blade temperature field with a single layer TBCs considering radiation. But for these FEM model, the surface conditions such as wall temperature and heat transfer coefficient are required to be assigned, which was difficult to measure. Currently the couple of gas flow and heat transfer has been used to calculate the blade temperature with the conjugate heat transfer method (CHT) at the fluid-solid interface (FSI). Bohn et al. [18–20], York et al. [21,22], and Dong et al. [23] studied the couple of gas flow and heat transfer using CHT. The major advantage of CHT is that it is required no boundary conditions on FSI.

But numerical simulation on actual turbine component with multilayered TBCs encounters troubles in two aspects. One is the geometry dimension difference between the thickness of TBCs and the component space scale. The other is the complex actual service condition. The big dimension difference tends to induce difficulties in constructing the multilayered blade and bring cumbersomeness in meshing and simulation. Yang et al. [24], Zhu et al. [25], and Tang et al. [26] have made good efforts to build the actual blade with multiple layers. Yang et al. [24] and Zhu et al. [25] ignored the gas flow environment. In the latest work [26], the computational fluid dynamics (CFD) and conjugate heat transfer method (CHT) were used to calculate the temperature of TBCs considering the cascade flow and heat transfer conditions.

However, under the couple of gas flow and heat transfer, insulation characteristics of TBCs and surface temperature fluctuation of the blade were paid little attention, but it is important to assess insulation of TBCs and stresses distribution in aerodynamic environment. Temperature dependences of the material properties and the thermal load history can result in unique residual stresses.

In this paper a cascade computational model with multilayered blade was built, coupling the gas flow, heat transfer, and inner cooling by CHT technology. The effects of inlet temperature, inner passage heat transfer coefficient, and coating thickness on TBCs insulation performances were studied. Meanwhile the surface temperature fluctuation was also discussed.

2. Numerical methods

2.1. Computational model and couple method

Aerodynamic cascade flow model and the stator blade (Mark II guide vane) originated from Hylton et al. [27]. The blade has a constant cross section and ten coolant passages (marked with Arabic numeral 1–10 in Fig. 1). In the paper, three layers (TC, TGO, BC) were added upon the outer surface. The thickness of BC and TGO are 150 μm and 10 μm, and TC is variable from 100 μm to 300 μm. The boundary conditions were kept consistent with the experiment (run number 42) [27]; the inner boundaries of coolant passages were listed in Table 1 [28]. But for exploring the influences of the variable aerodynamic conditions on insulation of TBCs, the inlet temperature of main flow and the heat transfer coefficients of ten passages were modified. Ideal gas assumption and mesh the fluid and solid domain in a uniform frame were adopted, keeping the grids node to node align at interface, as shown in Fig. 1. To resolve the viscous boundary layer, Y plus value (y^+) of the grids adjacent to the solid wall was less than 1. Mesh independence was done and a steady analysis was carried out using shear stress transport turbulence model considering boundary transition. For realizing the couple of gas flow and heat transfer,

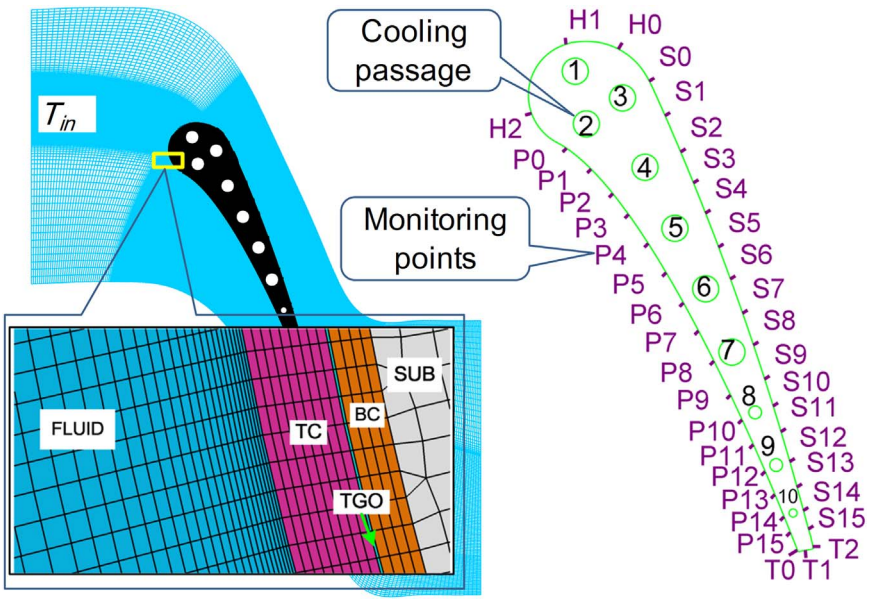

Fig. 1. Aerodynamic computational model and the local mesh (H0–H2, P0–P15, S0–S15, T0–T2 are the monitoring points at the head, the pressure side, the suction side, and the tail, respectively).

Table 1
Boundary conditions of the ten coolants [18].

Coolant number	Constant Temperature T (°C)	Heat transfer coefficient h_{cool} W/(m °C)
1	63.39	1943.67
2	53.27	1881.45
3	59.68	1893.49
4	65.86	1960.62
5	45.95	1850.77
6	42.58	1813.36
7	53.26	1871.88
8	86.83	2643.07
9	87.89	1809.89
10	141.85	3056.69

the solid domain should be assigned as the CHT domain. The two faces belong to fluid and solid domain at the FSI should be prescribed an energy conversation conjugate domain interface conditions, respectively. Conjugate conditions on the FSI provide continuity of the thermal fields by specifying the equalities of temperatures and heat fluxes of a solid body and a flow at the vicinity of interface: $T^+ = T^-$, $q^+ = q^-$.

The interface asperity between the solid layers is assumed to be perfect and no contact thermal resistance. The material thermal properties of the layers are temperature dependent and listed in Table 2. The samples listed in Table 3 were calculated through the coupled fluid and heat transfer method.

2.2. Validation of numerical method

For validating the methodology of the couple of gas flow and heat transfer currently utilized, we simulated the experiment (run number 42) without TBCs by keeping the boundary conditions consistent with the experiment, and then made a comparison with the experiment data shown in Fig. 2. Predicted non-dimensional surface temperature distribution was compared with experimental data in Fig. 2(a). The prediction showed good agreement with the experiment at pressure side ($-1 \le X_a/C_a \le 1$). And there was an over-estimation for $0.12 \le X_a/C_a \le 0.85$ at suction side. The maximum error was around 8.7%, which is acceptable to engineering application. Predicted pressure distribution was compared with experimental data in Fig. 2(a). The prediction exhibited excellent agreement with the experiment results, validating the aerodynamic of the model. It was supported that the numerical method used currently was validated properly.

3. Results and discussion

3.1. Temperature distribution of SUB

As shown in Fig. 3, SUB experienced non-homogeneous temperature distribution in each case; the lowest temperature

Table 2
Material properties [14,15].

Material	Temperature T (°C)	Thermal conductivity k (W/(m K))	Specific heat C (J/(kg K))	Density ρ (kg/m^3)	Thermal expansion α (10^{-6}/°C)
TBC	25	1.05	483	5650	9.68
	400				–
	800				9.88
	1000				10.34
TGO	25	25.20	857	3978	5.10
	400				–
	800				–
	1000				9.80
BC	25	4.30	501	7320	–
	400	6.40	592		12.50
	800	10.20	781		14.30
	1000	16.10	764		16.00
Substrate	25	11.56	582.2	7900	12.6
	400	18.38			14.00
	800	25.66			15.40
	1000	29.30			16.30

Table 3
Simulation cases.

Thickness of TC h_{TC} (μm)	Inlet temperature T_{in} (°C)			Heat transfer coefficient h_{cool} (W/(m °C))		
	727	1000	1300	$0.8h_{cool}$	$1.0h_{cool}$	$1.2h_{cool}$
100	√	√	√	√	√	√
200	√	√	√	√	√	√
300	√	√	√	√	√	√

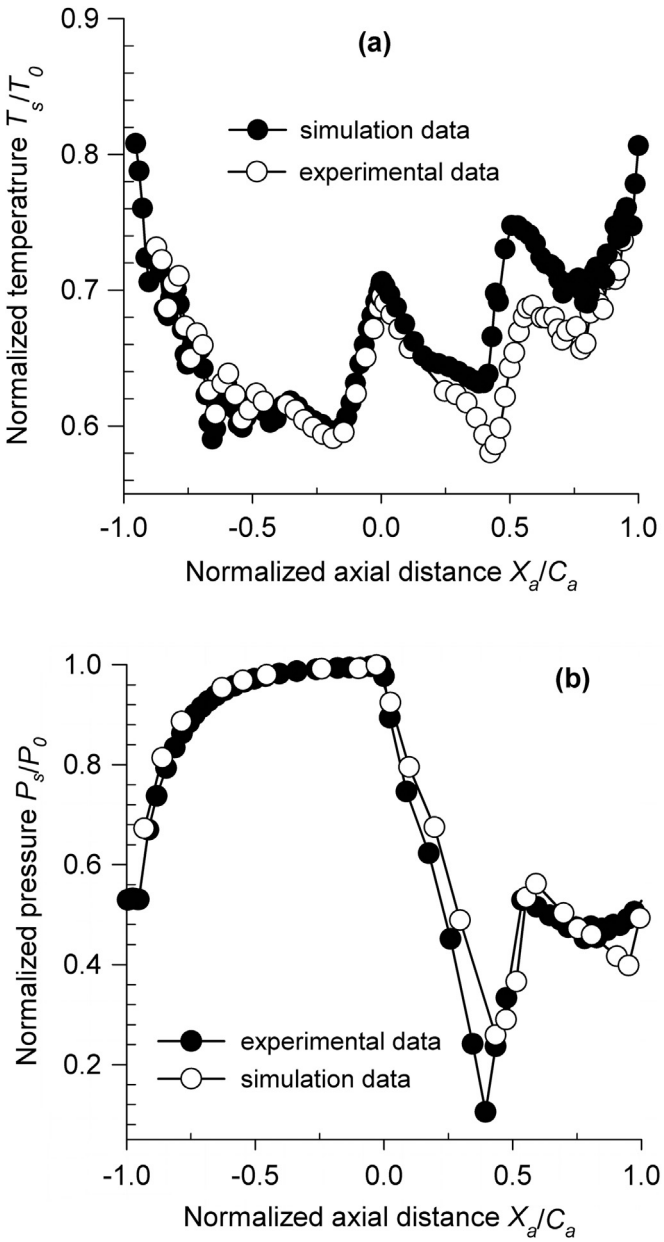

Fig. 2. Comparison with the experiment: (a) comparison of the temperature on surface (b) comparison of the pressure;

zone is at the head between the cooling passages 2 and 3; the highest temperature zone is at the tail; and the suction side is hotter than the pressure side. The tendency of the SUB temperature distribution and the positions of the highest and lowest temperature were consistent with the original experiment. It is a proof of the accuracy of our results. As T_{in} rising (Fig. 3(a)), the hotter zones (>600 °C) gradually broaden at the head, the suction side, and the tail for a given h_{TC}; and with h_{TC}

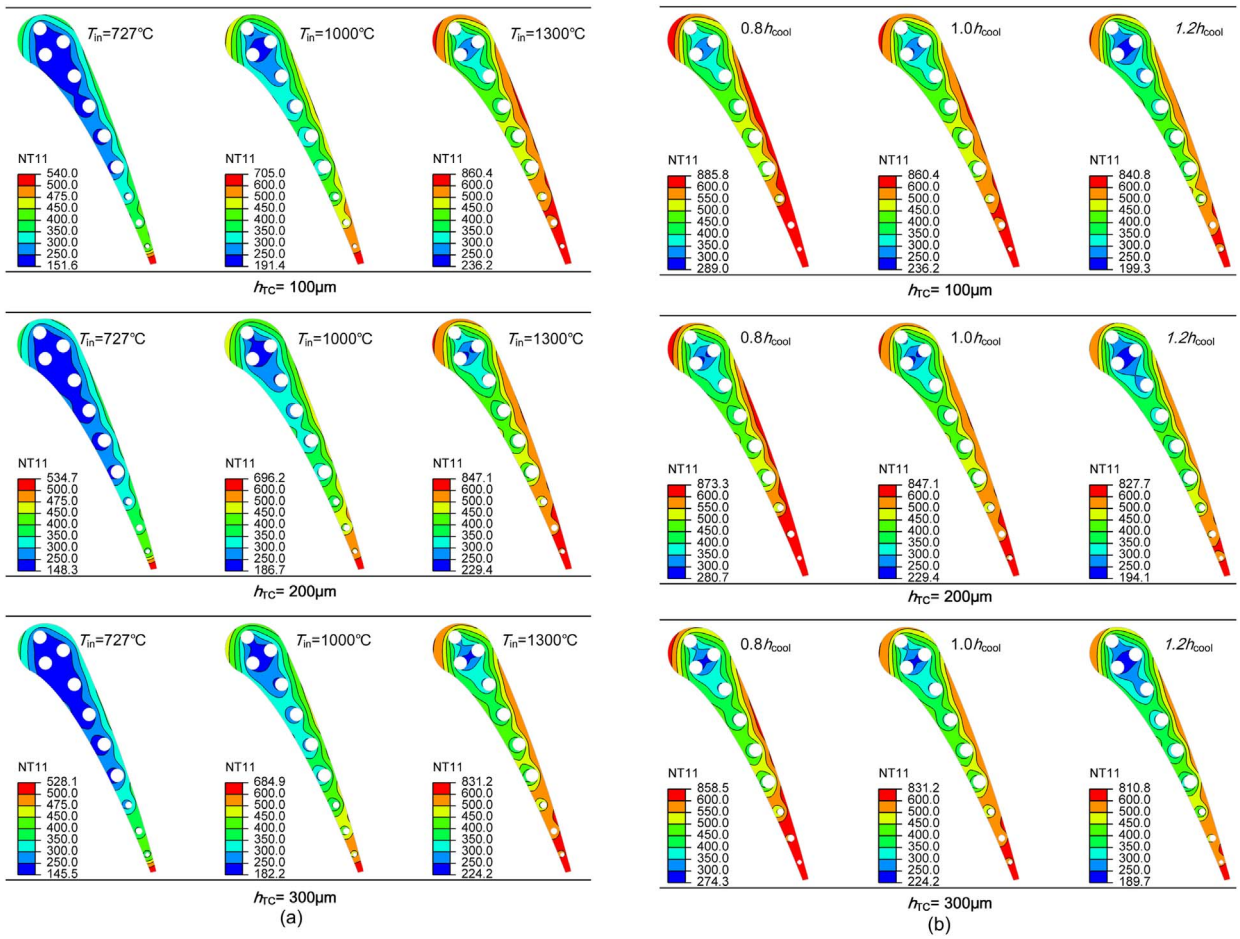

Fig. 3. SUB temperature distribution: (a) 1.0 h_{cool}, at different T_{in}; (b) T_{in} = 1300 °C, at different proportion of h_{cool}.

increasing, the hotter area is reduced by the coatings, especially at T_{in} = 1300 °C. On the other hand, as the proportion of h_{cool} increasing (Fig. 3(b)), the hotter range (> 600 °C) shrinks gradually for a given h_{TC}; and the hotter zones are visibly narrowed with rising of h_{TC}. These results suggest that the conditions of the main flow and inner coolant can affect the SUB temperature distribution, and thickened TC can decrease the hotter range.

The maximum, average and minimum temperature of SUB (T_{max}, T_{ave}, and T_{min}) are presented in Fig. 4. T_{max}, T_{ave}, and T_{min} all slope up with T_{in}. T_{max} has the fastest rate (Fig. 4(a)). T_{max}, T_{ave}, and T_{min} all slope down with the proportion of h_{cool}, and T_{min} slightly drops faster than others (Fig. 4(b)). It seems that T_{max} and T_{min} are more sensitive to T_{in} and h_{cool}, respectively. As shown in Fig. 4(a) and (b), a considerable decline of T_{ave} relative to the uncoated blade is brought in each cases. For example, in the cases h_{TC} = 100–300 μm at T_{in} = 1300 °C, T_{ave} are lowered by 41.0–113.3 °C than the case without coatings (Fig. 4(a)). The temperature reduction is similar to the reference [29], in which a full coating of ZrO_2-Y_2O_3 over a NiCoCrAlY bond coat was applied and obtained the metal temperature reductions ranged from 28 to 139 °C.

No significant drops of T_{max} can be found when TC is thin (h_{TC} = 100 μm), until h_{TC} reached 200 μm or more (Fig. 4(a) and (b)). Thus, we can conclude that the coated blade can benefit more in the decline of T_{ave} (ΔT_{ave}) than the decline of T_{max} (ΔT_{max}), compared to the uncoated case.

For the coated cases in Fig. 4(a), ΔT_{max} and ΔT_{ave} between different TC thicknesses both have a growth following the rising of T_{in}. At a given T_{in}, as h_{TC} thickening from 200 μm to 300 μm it acquires more effects on ΔT_{max} and ΔT_{ave} than the case thickening from 100 μm to 200 μm, presented in Table 4. On the other hand, ΔT_{max} and ΔT_{ave} versus the proportion of h_{cool} are relatively kept stable, and the average values are about 14.6 °C and 22.4 °C, respectively (Fig. 4(b)). It is likely that the flow conditions (T_{in}) impact TBCs insulation more than the cooling conditions (h_{cool}), and the thicker TBCs can benefit more than that of the thinner TBCs.

3.2. Temperature of TBCs

3.2.1. Average temperature on surface of TBCs

As show in Fig. 5, there are obvious differences in the average temperature on surface of TBCs ($T_{ave,sur}$). With TC

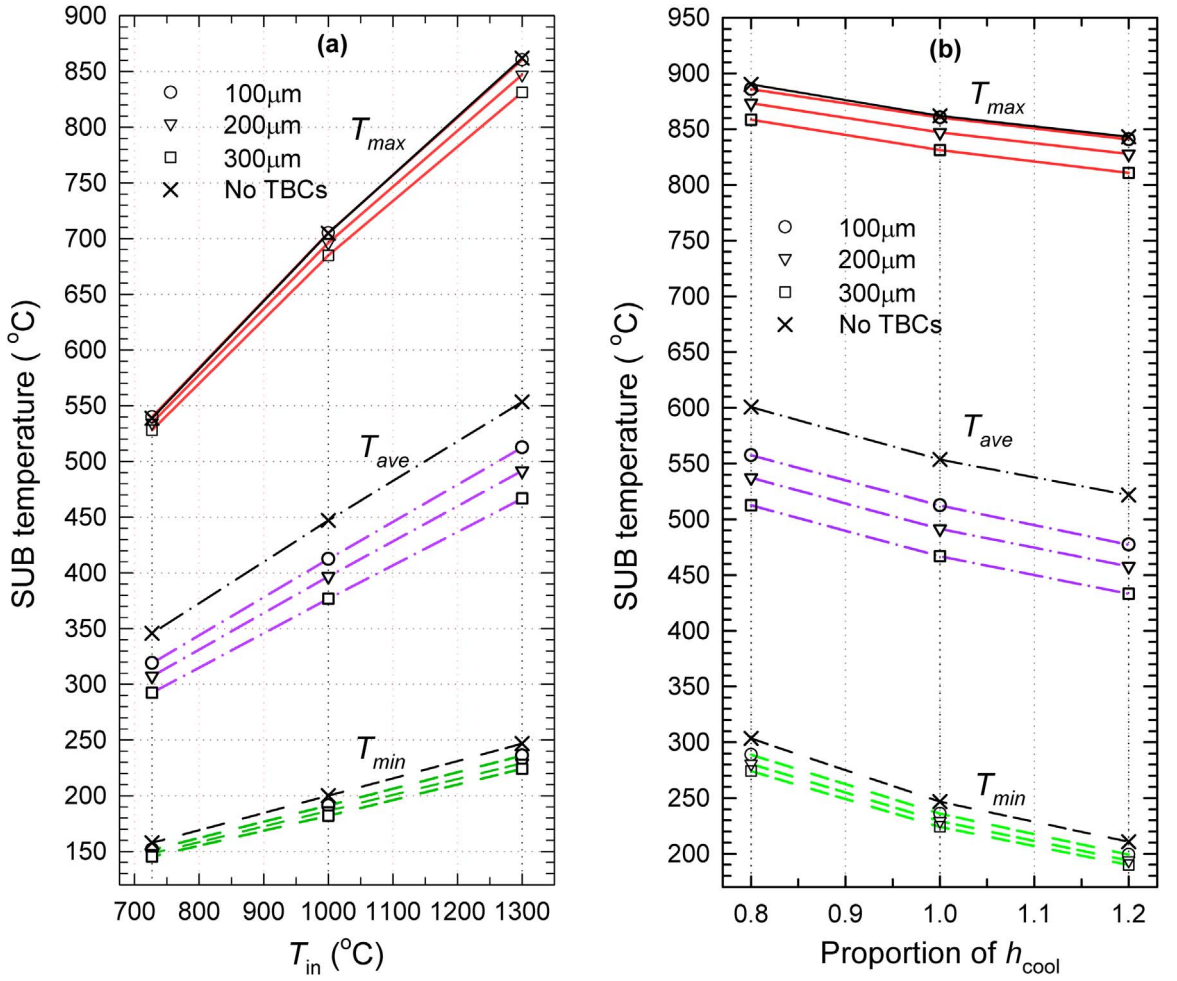

Fig. 4. Maximum, minimum, and average temperature of SUB: (a) 1.0 h_{cool}, at different T_{in}; (b) T_{in}=1300 °C, at different proportion of h_{cool}.

Table 4
Growth of ΔT_{max} and ΔT_{ave} with TC thickening (1.0 h_{cool}, at different Tin).

T_{in} (°C)	ΔT_{max}		ΔT_{ave}	
	First thickening (100–200 μm)	Second thickening (200–300 μm)	First thickening (100–200 μm)	Second thickening (200–300 μm)
727	5.1	6.6	11.6	15.0
1000	8.8	11.3	15.7	20.0
1300	13.3	15.9	21.0	24.7

thickening from 100 μm to 300 μm, the difference on $T_{ave,sur}$ reaches 15 °C at T_{in}=1300 °C (Fig. 5(a)). As T_{in} rises from 727 °C to 1300 °C, $T_{ave,sur}$ rises more than 440 °C (Fig. 5(a)). As the proportion rises from 0.8 to 1.2, $T_{ave,sur}$ descends more than 60 °C (Fig. 5(b)).

3.2.2. *Temperature deviation on surface of TBCs*

The temperature deviation (D) of on surface of TBCs was defined as the formula, (T_{sur}-$T_{ave,\ sur}$)/$T_{ave,\ sur}$*100%, where T_{sur} is the point temperature of the surface. As shown in Fig. 6, there is an evident temperature fluctuation on surface of TBCs. Generally, the negative value of D is about at the pressure side P1–P12, in where the peak value reaches nearly −30% at P8;

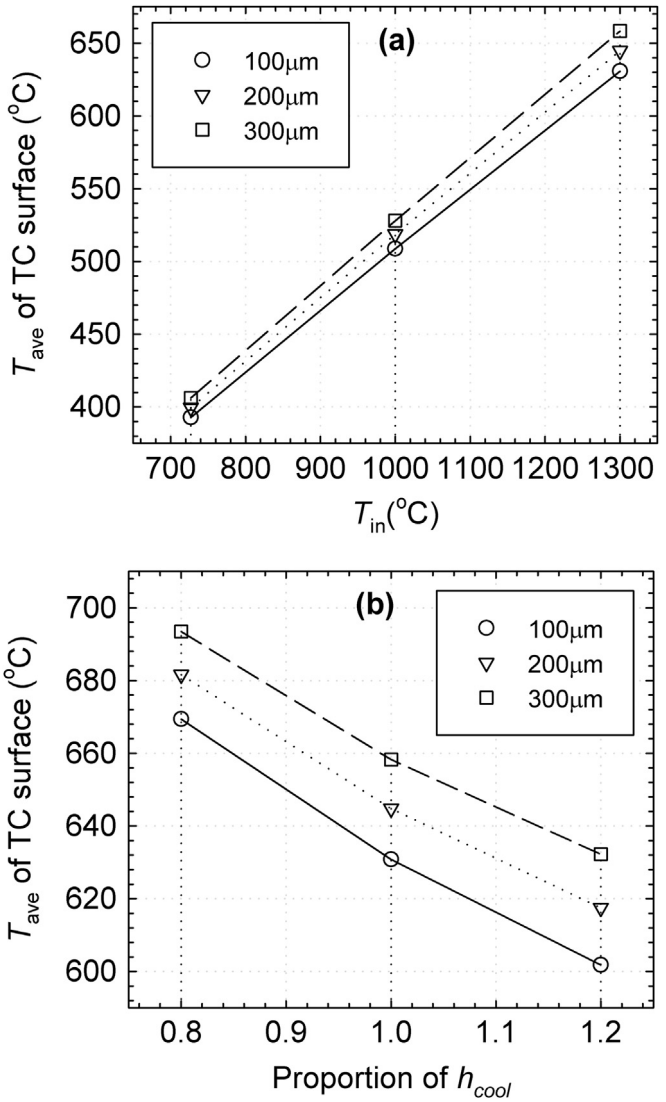

Fig. 5. Average temperature (T_{ave}) of TC surface: (a) 1.0 h_{cool}, at different T_{in}; (b) T_{in} = 1300 °C, at different proportion of h_{cool}.

the positive value of *D* is about at the whole tail and the suction side S2–S15, in where the peak value reaches nearly 40% at T1. It can be inferred that the suction side and the tail can produce thicker TGO than other parts in the higher temperature.

As shown in Fig. 6(a), the maximum difference of *D* between each case is less than 5.0%. With h_{TC} rising, *D* has a positive growth at S0–S14 and H0–H2, but a negative growth at P0–P15–T0–T2–S15. As shown in Fig. 6(b), there is a distinct difference of *D* at P12–P14, S0, and H0, where the peak value reaches 13.4%. With T_{in} rising, *D* has a positive growth at H1–H2–P0–P10 and S2–S14, and a negative growth at S0–S2 and P10–T0–T1. But at T1–T2–S15–S14 the difference of D is tiny. As shown in Fig. 6(c), the largest difference of *D* reaches 7.7% at the tail T1–T2. As the proportion rising, the difference of *D* has a positive growth at P0–P14, and a negative growth at H0–H2 and S0–S15–T2–T0–P15.

These results support that h_{TC} slightly affects the temperature fluctuation on surface, and the main flow conditions affect the surface fluctuation more than the inner cooling conditions.

3.2.3. *Temperature decline of TBCs*

The temperature decline (ΔT) from TBCs surface to the depth of 460 μm is shown in Fig. 7. There is a non-homogeneous distribution of ΔT around the blade. Generally, ΔT at the suction side and the head was higher than at the pressure side and the tail. The minimum value is about at T0, and the maximum value was about at S6.

As shown in Fig. 7(a), with h_{TC} rising, the growth of ΔT at the suction side and the head was more than other parts. The growth of ΔT with h_{TC} rising from 100 to 200 μm was a bit more than the rising from 200 to 300 μm. For example, the maximum growth of ΔT at S6 was 46.9 °C and 39.8 °C for the rising 100–200 μm and the rising 200–300 μm, respectively. As shown in Fig. 7(b), with T_{in} rising, the growth of ΔT at the suction side and the head was generally more than other parts.

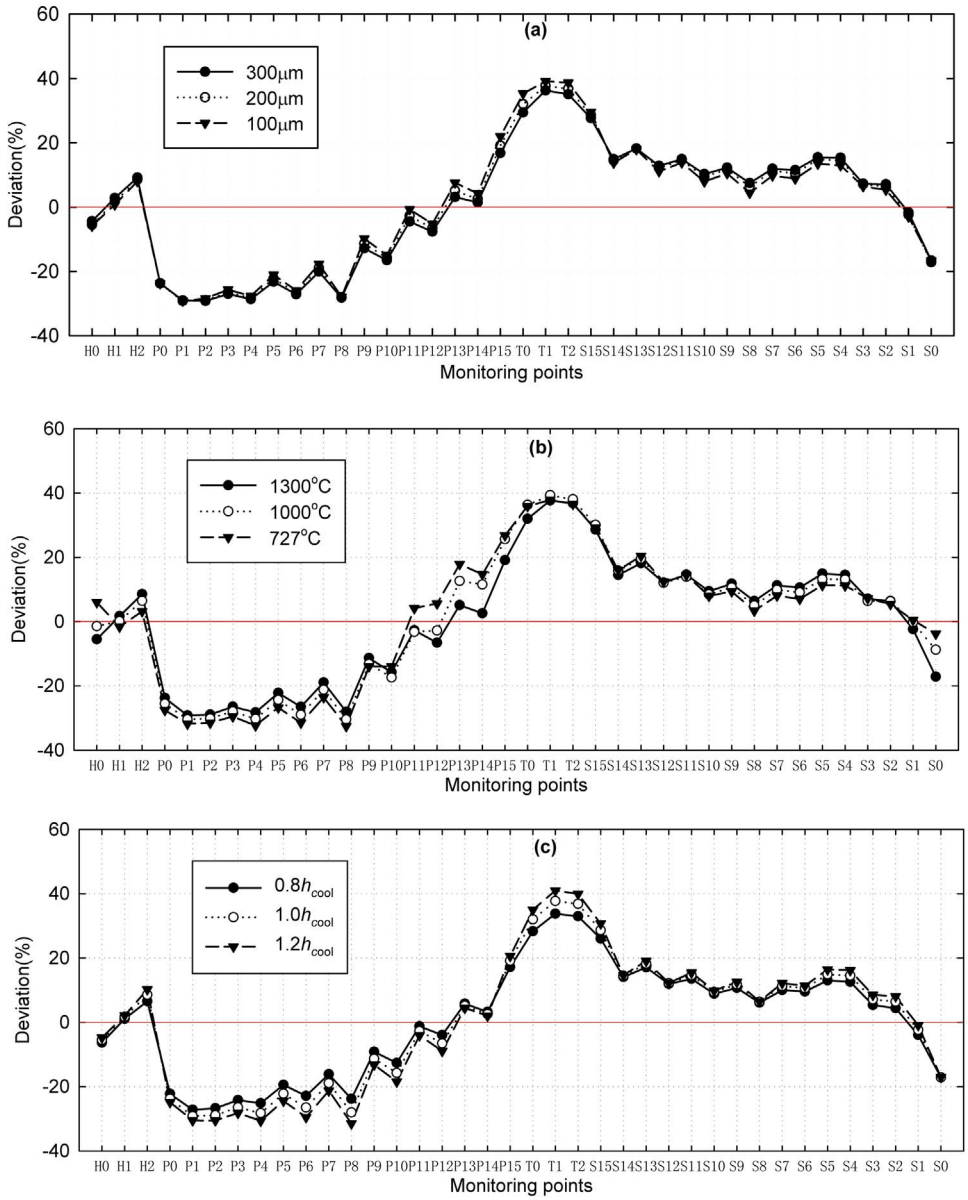

Fig. 6. TBCs Surface temperature deviation relative to the average value: (a) 1.0 h_{cool}, T_{in} = 1300 °C, at different h_{TC}; (b) 1.0 h_{cool}, h_{TC} = 200 μm, at different T_{in} (c) T_{in} = 1300 °C, h_{TC} = 200 μm, at different proportion of h_{cool}.

But at pressure side P12–P15, ΔT in the case T_{in} = 1300 °C is slightly lower than the case T_{in} = 1000 °C. As shown in Fig. 7(c), with the proportion of h_{cool} rising, the growth of ΔT was relatively small, and the suction side it slightly more than other parts.

Compared Fig. 7(a)–(c), the rising of h_{TC} exhibited more notable influence in ΔT, especially at the suction side and the head. As mentioned in Section 3.1, both the suction side and the tail are the hotter area. It can be infer that, to improve the hot-resistant, thickening the TBCs at the suction side may gain remarkable protection, but not so evident at the tail.

4. Conclusions

This paper has studied the insulation effects of TBCs through SUB and TC temperature distribution. The following conclusions have been obtained:

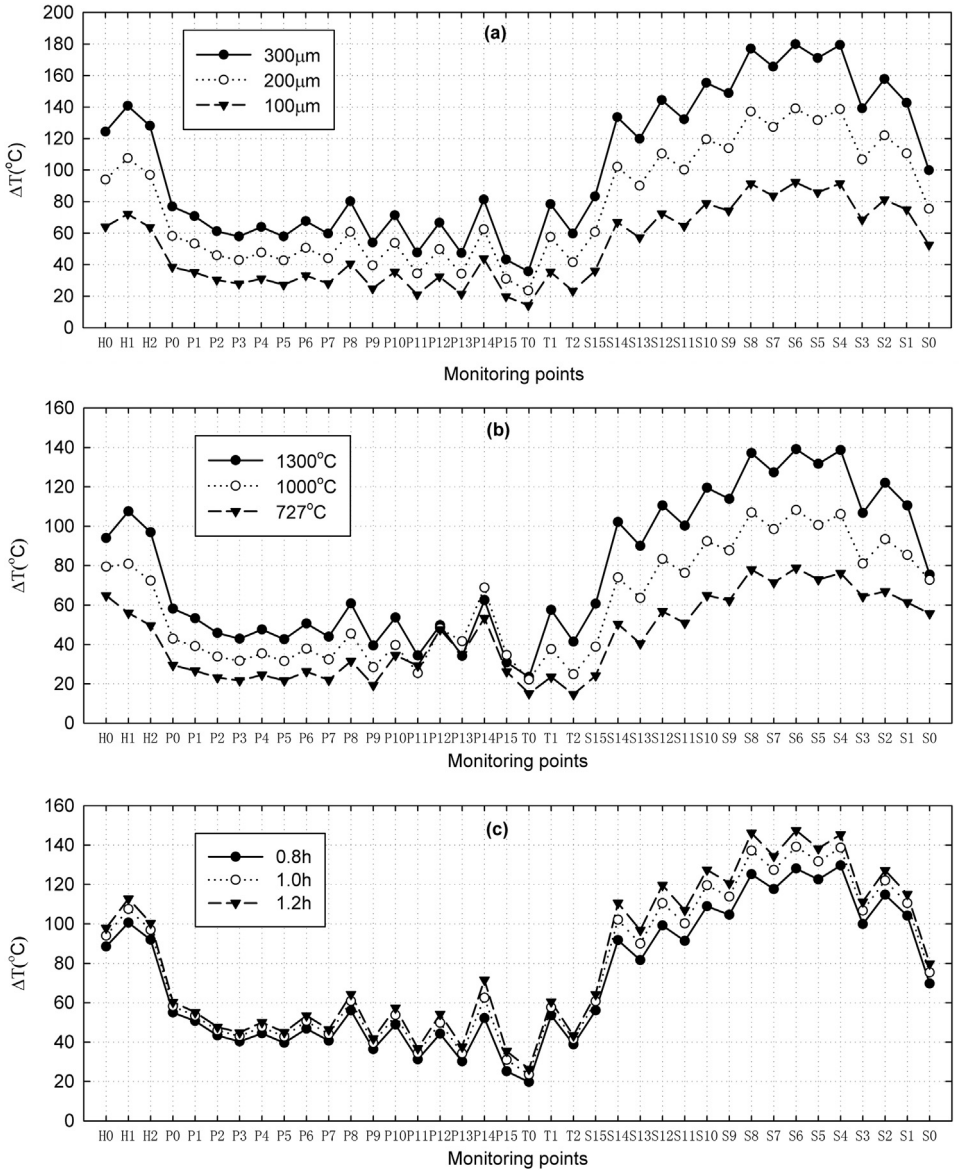

Fig. 7. Temperature decline across 460 μm depth from TBCs surface: (a) 1.0 h_{cool}, T_{in}=1300 °C, at different h_{TC}; (b) 1.0 h_{cool}, h_{TC}=200 μm, at different T_{in}; (c) T_{in}=1300 °C, h_{TC}=200 μm, at different proportion of h_{cool}.

(1) The coated blade can benefit more in ΔT_{ave} than in ΔT_{max}, compared to the uncoated case. The flow conditions (T_{in}), rather than the cooling conditions (h_{cool}), impacts the insulation effects of TBCs.
(2) Temperature fluctuation on TBCs surface is evident. h_{TC} can affect the temperature fluctuation on surface more slightly, but T_{in} can affect the fluctuation a bit more than h_{cool}. As these conditions varying, the variation of fluctuation is not constant all over the blade surface.
(3) There is a non-homogeneous distribution of ΔT around the blade. At the suction side and the head, ΔT was generally higher than at the pressure side and the tail. The rising of h_{TC} exhibit more notable influence in ΔT, but the influence is not consistent around the blade. We suggest that the sequential TBCs stresses simulation prescribe actual temperature distribution.

Acknowledgments

This work was supported by the National Natural Science Foundation of China (Grant No. 11305266). The authors gratefully acknowledge vice Professor Yu youhong and Wang Wenhua, Gas power teaching and Research Office, Navy university of engineering, China, for the software CFX operating.

References

[1] A.G. Evans, D.R. Mumm, J.W. Hutchinson, G.H. Meier, F.S. Pettit, Mechanisms controlling the durability of thermal barrier coatings, Prog. Mater. Sci. 46 (2001) 505–553.
[2] N.P. Padture, M. Gell, E.H. Jordan, Thermal barrier coatings for gas-turbine engine applications, Science 296 (2002) 280–284.
[3] A.G. Evans, J.W. Hutchinson, The mechanics of coating delamination in thermal gradients, Surf. Coat. Technol. 201 (2007) 7905–7916.
[4] E.P. Busso, J. Lin, S. Sakurai, A mechanistic study of oxidation-induced degradation in a plasma-sprayed thermal barrier coating system.: part II: life prediction model, Acta Mater. 49 (2001) 1529–1536.
[5] E.P. Busso, J. Lin, S. Sakurai, M. Nakayama, A mechanistic study of oxidation-induced degradation in a plasma-sprayed thermal barrier coating system.: part I: model formulation, Acta Mater. 49 (2001) 1515–1528.
[6] J. Aktaa, K. Sfar, D. Munz, Assessment of TBC systems failure mechanisms using a fracture mechanics approach, Acta Mater. 53 (2005) 4399–4413.
[7] M. Bäker, Finite element simulation of interface cracks in thermal barrier coatings, Comput. Mater. Sci. 64 (2012) 79–83.
[8] M. Bäker, J. Rösler, Simulation of crack propagation in thermal barrier coatings with friction, Comput. Mater. Sci. 52 (2012) 236–239.
[9] M. Białas, Finite element analysis of stress distribution in thermal barrier coatings, Surf. Coat. Technol. 202 (2008) 6002–6010.
[10] T.S. Hille, T.J. Nijdam, A.S.J. Suiker, S. Turteltaub, W.G. Sloof, Damage growth triggered by interface irregularities in thermal barrier coatings, Acta Mater. 57 (2009) 2624–2630.
[11] C.H. Hsueh, E.R. Fuller, Residual stresses in thermal barrier coatings: effects of interface asperity curvature/height and oxide thickness, Mater. Sci. Eng. A 283 (1999) 46–55.
[12] M. Ranjbar-far, J. Absi, G. Mariaux, D.S. Smith, Crack propagation modeling on the interfaces of thermal barrier coating system with different thickness of the oxide layer and different interface morphologies, Mater. Des. 32 (2011) 4961–4969.
[13] S. Widjaja, A.M. Limarga, T.H. Yip, Modeling of residual stresses in a plasma-sprayed zirconia/alumina functionally graded-thermal barrier coating, Thin Solid Films 434 (2003) 216–227.
[14] M. Ranjbar-Far, J. Absi, G. Mariaux, F. Dubois, Simulation of the effect of material properties and interface roughness on the stress distribution in thermal barrier coatings using finite element method, Mater. Des. 31 (2010) 772–781.
[15] M. Ranjbar-Far, J. Absi, G. Mariaux, S. Shahidi, Effect of residual stresses and prediction of possible failure mechanisms on thermal barrier coating system by finite element method, J. Therm. Spray Technol. 19 (2010) 1054–1061.
[16] T.A. Tietz, W.W. Koschel, Computer code for the calculation of the temperature distribution of cooled turbine blades, in: Proceedings of the 10th Symposium on Air Breathing Engines, 1991,1pp. 84–194.
[17] N.A. Kumar, S.R. Kale, Numerical simulation of steady state heat transfer in a ceramic-coated gas turbine blade, Int. J. Heat Mass Transf. 45 (2002) 4831–4845.
[18] D. Bohn, T. Heuer, K. Kusterer, D. Bohn, T. Heuer, K. Kusterer, Conjugate flow and heat transfer investigation of a turbo charger, J. Eng. Gas Turbines Power 127 (2005) 663–669.
[19] D. Bohn, J. Ren, K. Kusterer, Systematic investigation on conjugate heat transfer rates of film cooling configurations, Int. J. Rotating Mach. 2005 (2005) 211–220.
[20] K. Kusterer, T. Hagedorn, D. Bohn, T. Sugimoto, R. Tanaka, Improvement of a film-cooled blade by application of the conjugate calculation technique, J. Turbomach. 128 (2006) 572–578.
[21] W.D. York, J.H. Leylek, Three-dimensional conjugate heat transfer simulation of an internally-cooled gas turbine vane, in: Proceedings of ASME Turbo Expo 2003, Collocated with the 2003 International Joint Power Generation Conference, 2003, pp. 351–360.
[22] W.D. York, D.K. Walters, J.H. Leylek, A novel transition-sensitive conjugate methodology applied to turbine vane heat transfer, in: Proceedings of the ASME 2003 International Mechanical Engineering Congress and Exposition, 2003, pp. 55–65.
[23] P. Dong, Q. Wang, Z. Guo, H. Huang, G. Feng, Conjugate calculation of gas turbine vanes cooled with leading edge films, Chin. J. Aeronaut. 22 (2009) 145–152.
[24] L. Yang, Q.X. Liu, Y.C. Zhou, W.G. Mao, Finite element simulation on thermal fatigue of a turbine blade with thermal barrier coatings, J. Mater. Sci. Technol. 30 (2014) 371–380.
[25] W. Zhu, M. Cai, L. Yang, J.W. Guo, Y.C. Zhou, C. Lu, The effect of morphology of thermally grown oxide on the stress field in a turbine blade with thermal barrier coatings, Surf. Coat. Technol. 276 (2015) 160–167.
[26] W.Z. Tang, L. Yang, W. Zhu, Y.C. Zhou, J.W. Guo, C. Lu, Numerical simulation of temperature distribution and thermal-stress field in a turbine blade with multilayer-structure TBCs by a fluid–solid coupling method, J. Mater. Sci. Technol. 32 (2016) 452–458.
[27] L.D. Hylton, M.S. Mihelc, E.R. Turner, D.A. Nealy, R.E. York, L.D. Hylton, M.S. Mihelc, E.R. Turner, D.A. Nealy, R.E. York, Analytical and experimental evaluation of the heat transfer distribution over the surfaces of turbine vanes, AAS/Division of Dynamical Astronomy Meeting, 1983.
[28] D. Bohn, J. Ren, K. Kusterer, Cooling performance of the steam-cooled vane in a steam turbine cascade, ASME Turbo Expo 2005: Power for Land, Sea, and Air, 2005, pp. 217–226.
[29] S.M. Meier, D.K. Gupta, The Evolution of thermal barrier coatings in gas turbine engine applications, J. Eng. Gas Turbines Power 116 (1994) 250–257.